Valence fluctuations in thin films and the α and δ phases of Pu metal determined by 4*f* core-level photoemission calculations

G. van der Laan[1] and M. Taguchi[2]

[1]*Magnetic Spectroscopy Group, Diamond Light Source, Chilton, Didcot OX11 0DE, United Kingdom*
[2]*Excited Order Research Team, RIKEN SPring-8 Center, Sayo, Hyogo 679-5148, Japan*

The average number of 5*f* electrons making up the valence state in plutonium metal together with the electronic fluctuations on each metal site has been a recent subject of debate. For the δ phase of Pu, where compared to the α phase increased localization (more atomiclike character) leads to decreased overlap and volume increase, an *f* count close to either 5 or 6 has been proposed depending on the type of electronic structure calculation. In order to resolve the controversy, we analyze the Pu 4*f* photoemission spectrum, which displays well screened and poorly screened peaks that can be used as a measure for the degree of localization. A simple analytical two-level model already shows on general grounds that the *f* count for Pu must be between 5 and 5.5. Furthermore, we present detailed Anderson impurity model calculations including the full multiplet structure for Pu 4*f* photoemission, which are compared to previous experimental results obtained from 1 to 9 monolayers thin films of Pu on Mg and from Pu metal in the α and δ phases. The trend in the satellite to main peak intensity ratio as a function of the Pu layer thickness gives a clear indication that Pu metal has an $5f^5$ like ground state. For the Pu allotropes and thicker films an *f* count of 5.22 is obtained with a Coulomb interaction $U=4$ eV. The 5*f* fluctuations in Pu metal are very prominent and strongly material dependent. The calculations give a ground state with 9.6% f^4, 58.8% f^5, and 31.6% f^6 for the α phase and 5.7% f^4, 66.4% f^5, and 27.8% f^6 for the δ phase while for the thin films the amount of f^5 and the localization strongly increase with reduced thickness. The obtained findings are in agreement with recent electronic structure calculations for δ Pu using local-density approximation with dynamical mean-field theory and with the branching-ratio analysis of the Pu $N_{4,5}$ edge in electron-energy-loss spectroscopy.

I. INTRODUCTION

The huge environmental problems accompanying the waste products of the nuclear industry with the need to design safe storage demand an urgent need to understand the physical and chemical properties of compounds of the heavy elements such as uranium and plutonium. There are fundamental scientific questions as to the specific nature of 5*f* electrons in solids, which are not fully understood. Heavy-fermion behavior, the Kondo effect, anomalous superconductivity, valence fluctuations, and complex magnetic phases are among the characteristic features of correlated 5*f* electron systems.[1–4]

In actinide metals, the outer *s* and *d* electron orbitals are broad and overlap strongly and therefore show a metallic behavior. Conversely, the 5*f* orbitals, which have a smaller radius, display a more atomiclike behavior.[5] As the atomic number of the nucleus increases, the attractive electrostatic interaction increases, pulling the 5*f* electron orbitals closer to the atom. This causes the character of the 5*f* orbital to change from overlapping to nonoverlapping. Therefore, in the actinide series the lightest elements have itinerant 5*f* electrons, whereas the heavier actinides have atomiclike 5*f* electrons. The lighter elements display superconductivity while the heavier display magnetism, e.g., curium metal exhibits at high pressure an antiferromagnetically stabilized crystal structure.[6,7] Plutonium is placed at the boundary between delocalized (lighter elements, such as U and Np) and localized (heavier elements, such as Am and Cm). This unique place of Pu metal is responsible for its amazing amount of allotropes.[8,9] It makes Pu the most complex and anomalous element in the periodic table. The phase diagram of Pu metal contains seven allotropes, some with very complex crystal structures, not found in other metals, such as α Pu (the low-temperature phase) which has a complex monoclinic structure, whereas on the other hand δ Pu has a simple face-centered-cubic structure. The δ phase, which has a negative thermal-expansion coefficient and is stable at ambient pressure and between 592 and 724 K, has a ~25% larger atomic volume than the room-temperature α phase.[3]

For comparison, in the lanthanides, where the 4*f* orbitals are spatially less extended than the 5*f* in the actinides, the localization-delocalization transition occurs around Ce, making it the most remarkable element in the series. In lanthanides, high pressure gives an increased overlap leading to a delocalization.[10] Localization effects are also found in the 3*d* transition-metal series, e.g., thin films of Mn on Cu(110) show a dramatic change from delocalized for 4 monolayer (ML) to localized for submonolayer coverage.[11]

It is well established that the 5*f* occupation in the α phase of Pu metal is close to five electrons.[12–14] In the last few years, a controversy has arisen for δ-Pu metal concerning its *f* count (i.e., the average number of 5*f* electrons making up the valence state). Different electronic structure calculations predict different *f* counts, with local-density approximation (LDA)+U calculations giving 5.8 to 5.44 (Refs. 15–17) and dynamical mean-field theory (DMFT) calculations giving ~5.2 (Ref. 18). The LDA+DMFT method goes beyond the static model of LDA+U, which makes it an appropriate tool for studying 5*f* valence fluctuations.[19–21]

A critical test for the Pu electronic-structure calculation is the absence of any long-range magnetic order.[10,22] Localized electrons have a large exchange interaction, which aligns the spin and orbital moments. Most mean-field treatments that explain anomalies of δ Pu, such as its expanded volume, also predict that this phase is magnetic, which is experimentally not observed. As a matter of fact, no ordered moments have been observed for both α Pu and δ-stabilized Pu with magnetic-susceptibility measurements,[22] μSR,[23] and nuclear magnetic resonance.[24,25]

Already in 1975, Johansson and Rosengren[12] suggested a $5f^5$ like ground state, however, this solution converges to a magnetically ordered state. A convenient way to accommodate the absence of magnetic ordering in Pu metal was proposed in several recent publications (Refs. [15–17]) by choosing a configuration near $5f^6$. In this case, spin-orbit interaction splits the $5f$ shell into completely filled $f_{5/2}$ and empty $f_{7/2}$ states, with the local Coulomb interaction, U, enhancing this splitting, which results in nonmagnetic properties and a low specific heat capacity. Calculations using this model predict that the ground state of δ Pu is fairly similar to that of Am but less localized.[15,17] Due to the weak exchange interaction for a nonmagnetic $5f^6$ configuration the equilibrium volume of the δ phase is in agreement with the experiment.[16,26] However, the calculations in Refs. [15–17] are not consistent with the criterion of a similar occupation of the $5f$ states for all allotropes of metallic Pu and that this occupation is close to 5.[27] It was also suggested that the double-counting approximation in these calculations, the so-called around mean-field limit, is not appropriate for actinide materials.[27]

For a Pu $5f^5$ ground state the question of the equilibrium volume was addressed by Savrasov *et al.*[20,28] using LDA $+U+$DMFT. Depending on the value of the U parameter, i.e., the Slater integral $F^0(5f,5f)$ for the Coulomb interaction, DMFT is capable of reproducing both the Hubbard bands and the quasiparticle peak at the Fermi level. Using $U=4.0–4.5$ eV gives a double-minima shape of the total energy versus volume, with the minima corresponding to the experimental equilibrium volumes of the α and δ phases of Pu, i.e., corresponding to the itinerant and localized state of the $5f^5$ shell. In δ-Pu metal, DMFT leads to a nearly complete compensation of the spin and orbital contributions, with the local magnetic moments averaging out over short time scales.[18,28] Starting from an f^5 open-shell configuration, which is screened by the *spd* conduction electrons results in a Kondo resonance being formed at the Fermi level. DMFT explains the experimental $5f$ photoemission (PE),[18,29] the phonon spectrum,[21] and the large linear specific heat.[30]

A ground state with four f electrons treated as localized and one f electron as delocalized was proposed by Eriksson *et al.*[31,32] More sophisticated perhaps, in LDA with self-interaction correction (SIC), which corrects for the unphysical interaction of an electron with itself, the f electrons making up the valence are taken as core electrons and the remaining f electrons as itinerant. For the total energy of Pu metal LDA+SIC calculations give the configurations from f^0 to f^4 almost degenerate, with f^5 slightly higher in energy, and f^6 much higher in energy due to the Coulomb repulsion.[33] Thus while these calculations give an apparent f count of $\sim$2

for the metallic ground state of Pu metal, it gives f^6 in Am metal and f^7 in Cm metal as the lowest energy configuration.[33] Interestingly, the presence of nearly degenerate $5f$ levels in Pu metal indicates that a fluctuating valence state would be energetically favorable, which brings it in the realm of the Anderson impurity model.[34–36] In solids the f-electron occupation is noninteger and the Anderson impurity model can be used for arbitrary f count.

The f count can be experimentally obtained from x-ray absorption spectroscopy (XAS) or electron-energy-loss spectroscopy (EELS) using the sum-rule analysis of the branching ratio at the $N_{4,5}$ edge ($4d\rightarrow5f$ electric dipole transition), which gives the expectation value of the angular part of the $5f$ spin-orbit interaction per hole.[37–41] Measurement of the systematic trend in the branching ratio, i.e., the $I(N_5)/[I(N_5)+I(N_4)]$ intensity ratio, along the actinide series and comparison to multielectronic calculations provides evidence that the f count of Pu metal is close to five electrons.[3,7,41,42] Am metal with its closed relativistic subshell acts hereby as a beacon for f^6, where the branching ratio reaches a pronounced maximum, because the electric dipole transitions from the $4d_{3/2}$ core level (N_4 edge) are only allowed to the unoccupied $5f_{5/2}$ states, which are absent for $5f^6$.[42,43] While the branching ratio is a valuable tool to measure the f count, it is not sensitive to localization and valence fluctuations, unless the spin-orbit interaction is directly influenced by the localization.

Another powerful experimental tool is core-level PE. The $4f$ PE spectra of Pu display a well screened and poorly screened peak that can be used as a measure for the f count and the degree of localization. Satellite structure in PE arises due to a change in hybridization caused by the core-hole potential in the final state.[44,45] The satellite to main peak intensity is a function of the hybridization and the energy difference between the $5f$ configurations, which depends on the Coulomb interactions including its multipolar terms.

In this paper we give further evidence for a $5f^5$ like ground state for Pu metal in the α and δ phases. We present the results of Anderson impurity model calculations which give good agreement with the experimental results for thin films of Pu with different thicknesses. The experimental $4f$ PE spectra of 1, 2, 3, 5, and 9 ML Pu thin films on Mg have been previously published by Gouder *et al.*[46] and show a dramatic change in the satellite to main peak intensity with varying layer thickness. The satellite intensity, which is small for 9 ML, strongly increases for thinner films and becomes more intense than the main (well screened) peak for 2 and 1 ML Pu. This clearly indicates that there is a reduction in screening, i.e., increase in localization for thinner layers. A strong difference in the $4f$ PE spectrum is also observed between α and δ Pu metal.[47–49] The increased satellite structure in the δ phase can be related to a more localized $5f$ electronic structure.

The physics of the $5f$ electron systems at finite temperature is dominated by the phenomenon of electrons fluctuating between different configurations. It has been shown difficult—if not impossible—to account for the valence fluctuations using the electronic methodology of a one-electron mean-field description. The Anderson impurity model provides adequate tools to quantify the $5f$ fluctuations in Pu

metal. While we find that the $5f$ electron occupation is the same for both δ and α phases, the valence fluctuations are considerably different for both systems, evidencing the large change from localized to delocalized character.

The outline of the remainder of this paper is as follows. Section II gives a short overview of previous experimental results for $4f$ PE of actinide metals and, in particular, Pu metal. The theory follows in the next section. In Sec. III A we discuss the implications of the Hubbard model and in Sec. III B we describe the Anderson impurity model. In Sec. III C we present a simple model for a two-level system which allows us to derive some general results about the nature of the $5f$ ground state. In Sec. III D we give the theoretical details for the full multiplet calculations. The results of these calculations for thin films and the α and δ phases for Pu are presented and discussed in Sec. IV and the obtained f counts and f weights are compared with results reported elsewhere. Finally, the conclusions are given in Sec. V.

II. $4f$ CORE PHOTOEMISSION AS A PROBE FOR $5f$ LOCALIZATION

The peak structure of the $4f$ PE can be used to track the degree of $5f$ localization. In the literature one often finds that the main peak in the core-level PE spectrum is referred to as the well screened peak while the satellite peak is referred to as the poorly screened peak.[50] Although this correspondence is often correct, it is certainly not true in general. In Sec. III C we show for the case of a two-level system that a necessary and sufficient requirement for the main peak to be the screened peak is that the core-valence Coulomb interaction has to be larger than the charge-transfer energy between the levels in the initial state.

The experimental $4f$ PE spectra for α Th, α U, α Np, α and δ Pu, and α Am have been collected in Fig. 1. The large $4f$ spin-orbit interaction leads to two distinct manifolds, i.e., $4f_{7/2}$ and $4f_{5/2}$. The lighter metals (Th, U, and Np) exhibit asymmetric line shapes for the $4f_{7/2}$ and $4f_{5/2}$ peaks. In delocalized systems the peak asymmetry can be fitted by a Doniach-Sunjic line shape.[53] The asymmetry arises from the sudden creation of the core hole in PE, which gives rise to the creation of low-energy electron-hole pair excitations. The peak asymmetry becomes larger with increasing density of states at the Fermi level. The bulk of screening in the light actinides is performed by the delocalized $5f$ electrons[54] but this occurs to varying degrees. Looking along the light actinide metals, the satellite peaks are present in Th, entirely absent in U, and weak in Np. Th exhibits asymmetric peaks indicative of a delocalized metal.[51,55] Moser *et al.*[51] ascribed the observed satellite peaks in Th to sd conduction electrons while Fuggle *et al.*[50] ascribed them, in accord with the Gunnarsson and Schönhammer model,[45,56] to charge transfer from the Fermi level to unoccupied screening levels that are pulled down below the Fermi level when the core hole is created.

Pu and Am metals start to show broad peaks due to unresolved multiplet structure (Fig. 1). The degree of $5f$ delocalization is reflected by the satellite peaks at the high binding-energy (BE) side of the $4f_{7/2}$ and $4f_{5/2}$ structures. These
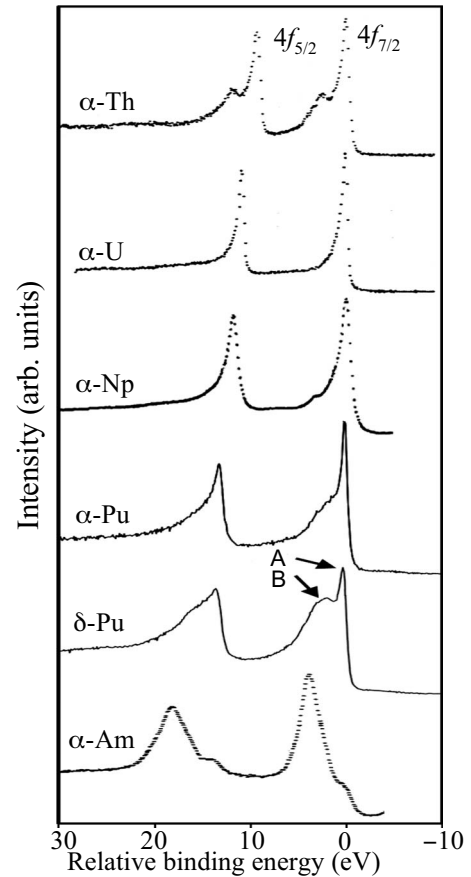
FIG. 1. The $4f$ PE spectra for metallic α Th (Ref. 51), α U (Ref. 51), α Np (Ref. 52), α and δ Pu (Refs. 47 and 48), and α Am (Ref. 43). The A and B indicate the main and satellite peaks, respectively. The large difference in the satellite peak intensity between α and δ Pu can be ascribed to a change in $5f$ localization. Intense satellite peaks on the high binding-energy side of the $4f_{7/2}$ and $4f_{5/2}$ peaks are indicative of a poor screening. In δ Pu the $5f$ states are more localized than in α Pu.

satellites are indicative of poor screening of the photoinduced core hole. Strong satellite structure is observed in α Pu,[57] which becomes more enhanced in δ Pu. The spectrum of Am consists almost entirely of satellite peaks, with a very small amount of weight at the position of the main peaks, which is characteristic for a localized system.

Figure 2 reproduces the experimental Pu $4f$ PE spectra for increasing Pu layer thickness (monolayers) on Mg metal measured by Gouder *et al.*[46] Strong changes in the spectra occur between a dominant main peak for 9 ML and a dominant satellite peak for 1 ML. The 9 ML spectrum resembles that of δ Pu, whereas the 1 ML spectrum appears very similar to that of Am in Fig. 1, where the $5f$ states are almost completely localized. The experimental spectra for the Pu $4f$ PE are compared with calculated results in Sec. IV.

III. THEORY

A. Hubbard model

The underlying physical picture of the electronic structure of the actinides is that the $5f$ electrons fluctuate among dif-
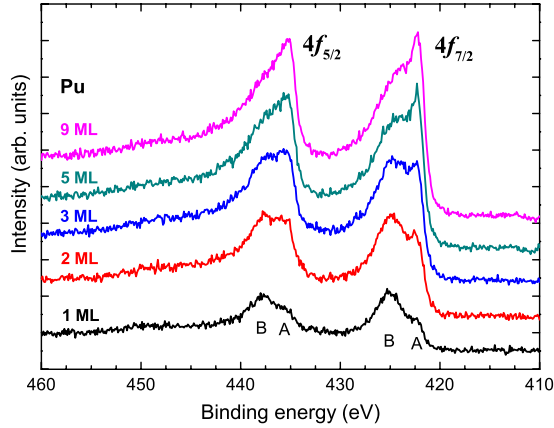
FIG. 2. (Color online) The Pu $4f$ PE spectra for Pu layer thicknesses from 1 to 9 ML, showing a gradual increase in the main to satellite intensity ratio with increasing layer thickness (Ref. 46). Spectra are shifted in vertical direction for clarity. The A and B indicate the main and satellite peaks, respectively. The spectrum for 9 ML Pu resembles that of δ-Pu metal, whereas 1 ML Pu resembles α Am (cf., Fig. 1).

ferent atomic configurations by exchanging electrons with a cluster. Quantum mechanically, for short periods of time, the electrons preserve their atomic character in a superposition of atomic valence states with different number of $5f$ electrons while at the same time also maintaining their metallic, delocalized hopping between neighboring sites. Correlations are strongest when the electrons are on the same atom while they are absent for itinerant electrons.

In the Hubbard model,[35,36] the electronic properties of a material are essentially determined by the two parameters, the transfer integral, V, which is inversely proportional to the electron hopping time $\Delta\tau = \hbar/V$, and the on-site $5f$ electron repulsion energy U, i.e., the Hubbard U [defined in Eq. (8)]. For small U/V the electrons are delocalized, whereas for large U/V the electrons are localized. In core-level spectroscopies the core hole with its attractive Coulomb potential can be used as an internal probe to study the electronic response.[44] In x-ray absorption, a core electron is excited from a core level into an unoccupied valence state, providing an element and site-specific probe for the local electronic structure.[58] However, the excited electron remains in the vicinity of the atom and is largely screening the core-hole potential. This means that it is more advantageous to use x-ray photoemission, where the core electron is excited into a continuum state, which has no interaction with the atom left behind.

The photoemission process is given in the sudden approximation by dipole transitions between the initial and final states [Eq. (4)]. If in the presence of a core hole the final state can be described by a linear combination of atomic $5f^n$ configurations, then only those $5f^n$ configurations in the initial state are involved in the transition that have overlap in wave function with the final state.[59] The initial state is (partly) delocalized, i.e., the electrons are hopping between different atoms, so that their f count fluctuates. However, the x-ray PE transition takes place in ~ 1 fs (10^{-15} s), on which time scale the $5f$ electrons are frozen. The result is an instan-

taneous picture over an ensemble average of atoms with different $5f^n$ configurations. Since the different configurations have different energies in the final state, they can be separated and their intensity determined. Such a model has been fruitfully used, e.g., for core PE from Ce metal and its intermetallics.[45,56] Effects due to the (indirect) interaction between f levels on different atoms are neglected.

In strongly localized electron systems, such as the $4f$ of Gd and Tb metals, the core-level PE is already well described by a single $4f^n$ configuration.[60–62] In the $3d$ transition-metal series, metallic nickel is a typical example of a correlated electron system, where the PE spectrum shows distinct satellite structure, which means that several $3d^n$ configurations are involved.[59] Other $3d$ metals, such as cobalt, have satellites that are substantially weaker,[63] which indicates that the satellite structure depends on the mixing of a large number of $3d^n$ configurations. When delocalization sets in, an asymmetric line shape starts to appear while the satellite structure diminishes.

A technical limitation in the calculation is the number of configurations that can be taken into account. In our Pu calculation this number is 3, which is sufficient for a physical description but more configurations are desired to obtain a better convergence. Ideally, the energy difference between the f^n configuration with lowest and highest energies in the initial state should be much larger than the mixing V. This condition is reasonably satisfied in the case of the thinner Pu films, but becomes more approximate for bulk Pu, and would be problematic for, say, Fe metal. The model is obviously less suited for valence photoemission due to the absence of a core hole, but still works well in the case of strongly localized states, such as heavier rare earths.[64]

It is interesting to contrast a correlated system against a one-electron model. In a one-particle band model (where $U = 0$) the probability that at an instantaneous moment an atom has n electrons (n=integer) is given by the binomial distribution[35,36]

$$P_n = \frac{z!}{n!(z-n)!}\left(\frac{c}{z}\right)^n\left(1 - \frac{c}{z}\right)^{z-n}, \qquad (1)$$

where z is the degeneracy, i.e., 14 for the f shell and c is the f count, i.e., the average number of electrons per atom. The distributions P_n are displayed in Fig. 3 (top) as a function of the f count. The standard deviation $\sigma = \sqrt{c(1-c/z)}$, shown by the dashed line in Fig. 3 (top), gives the frequency of the valence fluctuation. In Fig. 3 (bottom) we show the summed P_n, defined as $\Sigma_{n=0,k}P_n$ for each k as a function of the f count.

Returning to the Hubbard model, since electrostatic interactions will level out the electron charge distribution, atomic correlation effects reduce the charge fluctuation on each atom. Therefore, the f^n distributions become narrower with increasing U/V. For large U/V, we approach the atomic limit, where the fluctuations are suppressed and the f^n distributions become δ functions. Hence, it is clear that in metals fluctuations are the norm and static valences the exception.
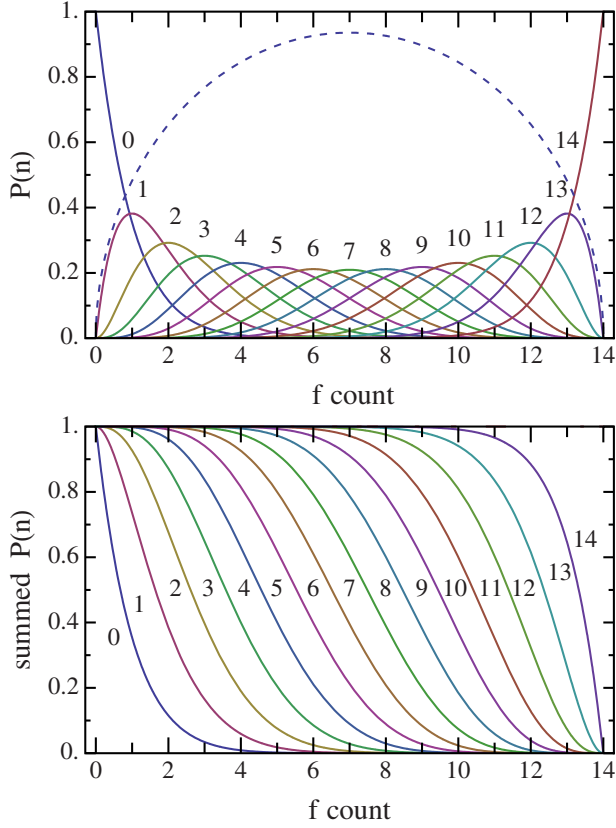
FIG. 3. (Color online) The f^n distributions in a one-electron model. Top panel: the binomial distribution P_n as a function of the f count, i.e., the average number of f electrons per atoms [cf., Eq. (1)]. The integer values n are indicated for each P_n curve. For an f metal without electron correlation the distributions give the probability that a particular atom has n electrons. The maximum of each P_n curve is at an f count of n. The integral under each curve is equal to 1. The standard deviation ($\times 1/2$) (dashed line) gives the frequency of the valence fluctuation. Correlation effects will narrow the width of each distribution and reduce the value of the standard deviation. Bottom panel: the summed binomial distributions, defined as $\Sigma_{n=0,k}P_n$, plotted for the indicated k values as a function of the f count. The f weights are given by the vertical distances between the curves. It can be verified that the total probability is always equal to 1.

B. Anderson impurity model calculations

The configuration interaction in the initial and final states is taken into account using a cluster model (local ligand-state version of the Anderson impurity model).[44,59] Consider a particular atomic site in a cluster of Pu atoms with a basis set of states $5f^n$ and states k, where k denotes a combination of appropriate symmetry of orbitals on the neighboring atoms. X-ray photoemission excites a core electron c to a continuum state ε, which has no spin-orbit, Coulomb and exchange interactions.

The electronic Hamiltonian $\mathcal{H}$ can be written as

$$\mathcal{H} = \mathcal{H}_{\text{atom}} + \mathcal{H}_{\text{cluster}} + \mathcal{H}_{\text{mix}} + \mathcal{H}_{\text{cont}} \qquad (2)$$

with

$$\mathcal{H}_{\text{atom}} = \sum_\nu E_{f\nu} f_\nu^\dagger f_\nu + \sum_\nu E_{c\nu} c_\nu^\dagger c_\nu$$

$$+ \sum_{\nu_1 \nu_2 \nu_3 \nu_4} \langle \nu_1 \nu_2 | Q | \nu_3 \nu_4 \rangle f_{\nu_1}^\dagger f_{\nu_2} c_{\nu_3}^\dagger c_{\nu_4}$$

$$+ \sum_{\nu_1 \nu_2 \nu_3 \nu_4} \langle \nu_1 \nu_2 | U | \nu_3 \nu_4 \rangle f_{\nu_1}^\dagger f_{\nu_2} f_{\nu_3}^\dagger f_{\nu_4}$$

$$+ \zeta_f \sum_{\nu_1 \nu_2} \langle \nu_1 | \ell \cdot s | \nu_2 \rangle f_{\nu_1}^\dagger f_{\nu_2} + \zeta_c \sum_{\nu_1 \nu_2} \langle \nu_1 | \ell \cdot s | \nu_2 \rangle c_{\nu_1}^\dagger c_{\nu_2},$$

$$\qquad (3a)$$

$$\mathcal{H}_{\text{cluster}} = \sum_\nu E_k k_\nu^\dagger k_\nu, \qquad (3b)$$

$$\mathcal{H}_{\text{mix}} = \sum_\nu V_\nu (f_\nu^\dagger k_\nu + k_\nu^\dagger f_\nu), \qquad (3c)$$

$$\mathcal{H}_{\text{cont}} = \sum_\nu E_\varepsilon \varepsilon_\nu^\dagger \varepsilon_\nu, \qquad (3d)$$

where $f_\nu^\dagger$, $c_\nu^\dagger$, $k_\nu^\dagger$, and $\varepsilon_\nu^\dagger$ (f_ν, c_ν, k_ν, and ε_ν) are the creation (annihilation) operators for the metal $5f$, metal core, cluster, and continuum electrons with energies E_f, E_c, E_k, and E_ε, respectively. The index ν labels all orbital and spin quantum numbers.

The Hamiltonian $\mathcal{H}_{\text{atom}}$ describes the single atom including the $5f$ and c electrons, which are split by spin-orbit interaction $\ell \cdot s$ with parameters ζ_{5f} and ζ_c, respectively, and intra-atomic electrostatic interactions with matrix elements $\langle Q \rangle$ and $\langle U \rangle$ determined by the Slater integrals. $\mathcal{H}_{\text{cluster}}$ describes the combinations of appropriate symmetry orbitals on adjacent sites, which are hybridized with the metal f states of the central atom as described by $\mathcal{H}_{\text{mix}}$, where V is the transfer integral (interatomic hopping). $\mathcal{H}_{\text{cont}}$ describes the continuum states.

The isotropic PE spectrum is expressed as

$$I(E_B) = \sum_{n,\nu} |\langle \Psi_n | \varepsilon_\nu^\dagger c_\nu | g \rangle|^2 \delta(E_B - E_{\underline{c},n} + E_g), \qquad (4)$$

where E_B is the binding energy and $|g\rangle$ and $|\Psi_n\rangle$ are the initial and the final states with energy E_g and $E_{\underline{c},n}$, respectively. The underscore denotes a hole state. If we restrict us to the configurations $5f^n$ with $n=4,5,6$, these states are given as

$$|g\rangle = \alpha |5f^4 k^2\rangle + \beta |5f^5 k\rangle + \gamma |5f^6\rangle, \qquad (5a)$$

$$|\Psi_n\rangle = \alpha_n |\underline{c} 5f^4 k^2 \varepsilon\rangle + \beta_n |\underline{c} 5f^5 k \varepsilon\rangle + \gamma_n |\underline{c} 5f^6 \varepsilon\rangle, \qquad (5b)$$

where hybridization mixes the configurations. α, β, and γ are the coefficients of the ground-state wave function normalized such that $\alpha^2 + \beta^2 + \gamma^2 = 1$. The squares of these coefficients give the relative weights of the corresponding configurations in the ground state. α_n, β_n, and γ_n are the coefficients of the final-state wave function Ψ_n, having a normalization $\alpha_n \alpha_m + \beta_n \beta_m + \gamma_n \gamma_m = \delta_{nm}$. In the following, we will omit k and ε in the notation of the configurations since this does not lead to any ambiguity.

Equation ([5a]) allows a nonmagnetic ground state, where f^6 imposes a singlet ground state on the hybridized state, making it nonmagnetic. The magnetic moments of the f^5 and f^4 are compensated by those of k and k^2, respectively. This is called Kondo shielding, where the neighboring conduction electrons cloak the local magnetic moment that should be on the Pu.

The total energy for an atomic configuration ℓ^n in the absence of hybridization (i.e., in the limit of $V \to 0$) is given as

$$E_n \equiv n\epsilon_\ell + \frac{1}{2}n(n-1)U, \tag{6}$$

where ϵ_ℓ represents the kinetic energy of a single electron in the ℓ shell and U is the intra-atomic Coulomb interaction, the so-called Hubbard U. From this the excitation spectrum is obtained as

$$\epsilon_n = E_{n+1} - E_n = \epsilon_\ell + nU \tag{7}$$

and U satisfies the relation

$$E_{n+1} + E_{n-1} - 2E_n = U, \tag{8}$$

which is consistent with the definition used by, e.g., Savrasov *et al.*[20] and Shim *et al.*[18]

For the final state in the presence of a core hole with energy $\epsilon_{\underline{c}}$ the total energy of the configuration $\underline{c}\ell^n$ is

$$E_{\underline{c},n} = \epsilon_{\underline{c}} + n\epsilon_\ell + \frac{1}{2}n(n-1)U - nQ, \tag{9}$$

where Q is the core-valence Coulomb interaction.

For our case it is convenient to set the energy $E_5 = 0$ and to define the charge-transfer energy $\Delta \equiv E_6 - E_5 = \epsilon_\ell + 5U$. Then the initial-state configurations have the relative energies

$$E(5f^4) = -\Delta + U, \tag{10a}$$

$$E(5f^5) = 0, \tag{10b}$$

$$E(5f^6) = \Delta. \tag{10c}$$

From Eq. ([9]) the final-state configurations have *relative* energies

$$E(\underline{c}5f^4) = E(5f^4) + Q = -\Delta + U + Q, \tag{11a}$$

$$E(\underline{c}5f^5) = E(5f^5) = 0, \tag{11b}$$

$$E(\underline{c}5f^6) = E(5f^6) - Q = \Delta - Q. \tag{11c}$$

The energies of the initial- and final-state configurations are located on parabolic curves, as can be seen from Eqs. ([6]) and ([9]). The (fractional) f counts corresponding to the state of minimum energy are

$$\langle n \rangle_{\text{initial}} = \frac{11}{2} - \frac{\Delta}{U}, \tag{12a}$$

$$\langle n \rangle_{\text{final}} = \frac{11}{2} - \frac{\Delta}{U} + \frac{Q}{U}, \tag{12b}$$

for the initial and final states, respectively. Therefore, in order to fully screen the final-state core hole requires $\langle n \rangle_{\text{final}} - \langle n \rangle_{\text{initial}} = Q/U$ additional $5f$ electrons. Typical values for the Coulomb interactions are $1 < Q/U < 1.25$. How much screening charge can be mobilized within the core-hole lifetime (~ 1 fs) depends on the size of the $5f$ hopping.

C. Illustrative two-level model for core-level photoemission

We first present a simple analytical model that qualitatively explains the relative satellite intensity of the core PE and the $5f$ screening as a function of the hybridization. With this model we will already be able to draw some important conclusions regarding the f count, without having to resort to detailed calculations of the spectra. The important point here is that we do not *a priori* assume any definite character of the ground state. We show that if the energy positions of the two main configurations f^n and f^{n+1} are reversed in the PE final state, due to the Coulomb interaction with the core hole, then the ground state must have predominantly f^n character.

In the sudden approximation the photoemission intensities I_n corresponding to the final states Ψ_n can be obtained using Eqs. ([4]) and ([5]) as

$$I_n = |\langle \Psi_n | \varepsilon^\dagger c | g \rangle|^2 = (\alpha\alpha_n + \beta\beta_n + \gamma\gamma_n)^2, \tag{13}$$

hence the peak intensity depends on the wave-function coefficients of the initial and final states. In order to derive useful analytical expressions we will consider only the two main configurations, and omit configurations of higher energy, as well as multiplet and band structure. We will make no *a priori* assumption of the $5f$ count.

The Hamiltonian in matrix form for a ground state consisting of two configurations is

$$\mathcal{H} = \begin{vmatrix} 0 & V \\ V & \Delta \end{vmatrix} \tag{14}$$

with basis states $|\ell^n\rangle$ and $|\ell^{n+1}\rangle$ that have an energy difference $\Delta = E(\ell^{n+1}) - E(\ell^n)$ and mixing (hybridization) $V = \langle \ell^{n+1} | \mathcal{H} | \ell^n \rangle$, where we choose $V > 0$. The hybridized ground state is

$$|g\rangle = \cos\theta |\ell^n\rangle + \sin\theta |\ell^{n+1}\rangle \tag{15}$$

with

$$\tan 2\theta = \frac{2V}{\Delta}. \tag{16}$$

Thus the angle θ is a measure for the hybridization in the ground state ($0 < \theta < \pi/2$). We can distinguish the following two cases: (i) $\Delta > 0$, where $0 < \theta < \pi/4$ and $|\ell^n\rangle$ has the lowest energy and (ii) $\Delta < 0$, where $\pi/4 < \theta < \pi/2$ and $|\ell^{n+1}\rangle$ has the lowest energy.

For the final state, after creation of a core hole, the Hamiltonian in matrix form is

$$\mathcal{H} = \begin{vmatrix} 0 & V \\ V & \Delta - Q \end{vmatrix} \qquad (17)$$

with basis states $|\underline{c}\ell^n\rangle$ and $|\underline{c}\ell^{n+1}\rangle$ that have an energy difference $E(\underline{c}\ell^{n+1}) - E(\underline{c}\ell^n) = \Delta - Q$. For simplicity we take the mixing V the same as in ground state. Since the Coulomb interaction between the core hole and $5f$ electrons is attractive, $Q > 0$. The final states corresponding to the main (m) and satellite (s) peaks are

$$|\Psi_m\rangle = \cos\theta' |\underline{c}\ell^n\rangle + \sin\theta' |\underline{c}\ell^{n+1}\rangle, \qquad (18a)$$

$$|\Psi_s\rangle = \sin\theta' |\underline{c}\ell^n\rangle - \cos\theta' |\underline{c}\ell^{n+1}\rangle \qquad (18b)$$

with

$$\tan 2\theta' = \frac{2V}{\Delta - Q} \qquad (19)$$

so that θ' is a measure for the hybridization in the final state ($0 < \theta' < \pi/2$). We define the main peak as the peak arising from the bonding state and consequently it has lower energy than the satellite peak, i.e.,

$$E(\Psi_s) - E(\Psi_m) \equiv \sqrt{(\Delta - Q)^2 + 4V^2}, \qquad (20)$$

is always positive.

In the sudden approximation, the satellite to main peak intensity ratio is obtained using Eq. (13) as[44]

$$\frac{I_s}{I_m} = \left| \frac{\langle \Psi_s | \varepsilon^\dagger c | g \rangle}{\langle \Psi_m | \varepsilon^\dagger c | g \rangle} \right|^2 = \left(\frac{\cos\theta \sin\theta' - \sin\theta \cos\theta'}{\cos\theta \cos\theta' + \sin\theta \sin\theta'} \right)^2$$

$$= \tan^2(\theta' - \theta). \qquad (21)$$

The peak corresponding to the final state with the largest amount of ℓ electrons, i.e., with the largest $|\underline{c}\ell^{n+1}\rangle$ character, is called the well screened peak while the other peak is the poorly screened peak. The well screened peak is always pulled down in energy by an amount Q [cf., Eq. (17)]. However, whether the well screened peak is either the main or the satellite peak depends on the sign of $\Delta - Q$. Therefore, we can distinguish the following two cases:

(i) *No level reversal between ground and final states*, $\Delta - Q > 0$, where $0 < \theta' < \pi/4$ and $E(\underline{c}\ell^{n+1}) > E(\underline{c}\ell^n)$, so that the main peak has primarily $|\underline{c}\ell^n\rangle$ character and is therefore the poorly screened peak. Consequently, the satellite peak has mainly $|\underline{c}\ell^{n+1}\rangle$ character and is the well screened peak.

(ii) *Level reversal between initial and final states*, $\Delta - Q < 0$, where $\pi/4 < \theta' < \pi/2$ and $E(\underline{c}\ell^n) > E(\underline{c}\ell^{n+1})$, so that the main peak has primarily $|\underline{c}\ell^{n+1}\rangle$ character and is therefore the well screened peak.

Furthermore, it is useful to recognize the following symmetry. In the ground state, Eqs. (15) and (16) are invariant under simultaneous interchange of $|\ell^n\rangle \Leftrightarrow |\ell^{n+1}\rangle$, $\theta \Leftrightarrow \pi/2 - \theta$, and $\Delta \Leftrightarrow -\Delta$. In the final state, Eqs. (18) and (19) are invariant under simultaneous interchange of $|\underline{c}\ell^n\rangle \Leftrightarrow |\underline{c}\ell^{n+1}\rangle$, $\theta' \Leftrightarrow \pi/2 - \theta'$, and $\Delta - Q \Leftrightarrow Q - \Delta$.

Using the above symmetry conditions we obtain for the satellite to main peak intensity ratio,

$$I_s/I_m = R \quad \text{for} \ \ \Delta(\Delta - Q) > 0, \qquad (22a)$$

$$I_s/I_m = R^{-1} \quad \text{for} \ \ \Delta(\Delta - Q) < 0, \qquad (22b)$$

where R is a function given by the parameters appearing in the Hamiltonians for initial and final states,

$$R = f(\Delta, V, Q). \qquad (23)$$

Using that $Q > 0$, the conditions for Eq. (22) can be rewritten as

$$I_s/I_m = R \quad \text{for} \ \ (\Delta < 0) \cup (\Delta > Q), \qquad (24a)$$

$$I_s/I_m = R^{-1} \quad \text{for} \ \ 0 < \Delta < Q. \qquad (24b)$$

R is a complicated expression but we can write it as a series expansion in V. For small hybridization (i.e., $V \ll |\Delta|$ and $V \ll |\Delta - Q|$), Eqs. (16) and (19) can be approximated in the different cases as

$$\theta = V/\Delta \quad \text{for} \ \ \Delta > 0, \qquad (25a)$$

$$\theta = V/\Delta + \pi/2 \quad \text{for} \ \ \Delta < 0, \qquad (25b)$$

$$\theta' = V/(\Delta - Q) \quad \text{for} \ \ \Delta - Q > 0, \qquad (25c)$$

$$\theta' = V/(\Delta - Q) + \pi/2 \quad \text{for} \ \ \Delta - Q < 0, \qquad (25d)$$

and substitution into Eq. (21) gives

$$R = \frac{Q^2 V^2}{\Delta^2 (\Delta - Q)^2} - \frac{2Q^2 (2\Delta - Q)^2 V^4}{\Delta^4 (\Delta - Q)^4} + O[V]^6. \qquad (26)$$

According to Eqs. (24b) and (26), I_m/I_s is in lowest order proportional to the square of V when $|\ell^n\rangle$ and $|\underline{c}\ell^{n+1}\rangle$ have the lowest energy in initial and final states, respectively, i.e., when level reversal takes place between initial and final states.

In all other cases, according to Eqs. (24a) and (26), I_s/I_m is in lowest order proportional to the square of V, thus when $|\ell^{n+1}\rangle$ has the lowest ground-state energy or when $|\ell^n\rangle$ and $|\underline{c}\ell^{n+1}\rangle$ have the lowest energy in initial and final states, respectively. In this case there is no level reversal between initial and final states.

We will now apply this to the measured Pu spectra. We assume that Δ and U remain approximately constant for the thin films and allotropes of Pu. We can furthermore expect the localization to decrease, i.e., V increases, with increasing Pu layer thickness and also, as is generally accepted, the localization decreases going from the δ to α phase. Therefore, the experimental PE spectra in Figs. 1 and 2 show that I_m/I_s increases with increasing V, which corresponds to the scenario that $0 < \Delta < Q$. Hence, Δ is positive and $\Delta - Q$ is negative, which means an energy reversal between the levels in the initial and final states. From the condition that $\Delta > 0$ we reach the important conclusion that $E(\ell^{n+1}) > E(\ell^n)$. This means that the f count is between n and $n+0.5$ while it cannot be between $n+0.5$ and $n+1$, where n is an integer. We now have to decide which are the two main configurations in the case of Pu metal. Assuming an f count in Pu metal between $n=6$ and 6.5 would not be realistic since the heavier neighbor metals Am and Cm are close to f^6 and f^7, respectively,[3] and Pu should have less electrons. Therefore,

TABLE I. Atomic Hartree-Fock values of the Slater integrals F^k and G^k, and the spin-orbit parameters ζ in eV for the initial- and final-state configurations in the photoemission process, Pu $5f^n \rightarrow 4f^{13}5f^n\varepsilon$, calculated using Cowan's code.

		$n=4$	$n=5$	$n=6$
$5f^n$ configuration	$F^2(5f,5f)$	10.282	9.700	8.996
	$F^4(5f,5f)$	6.741	6.317	5.810
	$F^6(5f,5f)$	4.955	4.628	4.241
	$\zeta(5f)$	0.334	0.307	0.279
$4f^{13}5f^n$ configuration	$F^2(5f,5f)$	11.162	10.687	10.148
	$F^4(5f,5f)$	7.370	7.020	6.626
	$F^6(5f,5f)$	5.439	5.167	4.862
	$\zeta(5f)$	0.395	0.368	0.342
	$\zeta(4f)$	3.538	3.538	3.537
	$F^2(4f,5f)$	6.116	5.787	5.445
	$F^4(4f,5f)$	2.703	2.536	2.366
	$F^6(4f,5f)$	1.680	1.573	1.464
	$G^0(4f,5f)$	1.632	1.531	1.427
	$G^2(4f,5f)$	2.059	1.927	1.793
	$G^4(4f,5f)$	1.614	1.509	1.404
	$G^6(4f,5f)$	1.264	1.182	1.099

the fact that the main to satellite intensity ratio increases with increasing hybridization leaves no other conclusion than that the f count is between 5 and 5.5. This means that from the trend in the PE satellite we can exclude a ground state in which the main configuration is f^6 with some f^5 mixed in, as has been proposed in some theoretical studies.[15–17]

Of course, the real situation includes in addition also other f^n configurations at higher energies, notably a small amount of f^4, as well as multiplet structure, which gives a wide energy spread of the levels in each configuration, thereby affecting the peak intensity ratio. To take this into account the cluster model introduced in Sec. III B will be used to evaluate the PE in a more accurate way in the following sections.

D. Full multiplet calculations

In the cluster model, the Hamiltonians [Eq. (2)] for the initial and final states [Eq. (5)] are calculated in SO_3 symmetry using Cowan's code,[65] neglecting crystal-field interaction and band-structure dispersion. The code calculates the wave functions in intermediate coupling using the atomic Hartree-Fock with relativistic corrections.[66] The obtained Hartree-Fock values of the Slater integrals and spin-orbit parameters for initial and final states are listed in Table I. The photoemission is calculated using Eq. (4) with the Slater integrals empirically reduced to 80% to include intra-atomic relaxation effects.[67] The number of levels for each configuration ℓ^n is equal to the binomial $(4\ell+2,n)$, which becomes quite large, e.g., in the PE transition $5f^6 \rightarrow 4f^{13}5f^6\varepsilon$ there are 3003 and 48 048 levels in the initial and final states, respectively.

The effects of configuration dependent hybridization are taken into account by introducing two reduction factors
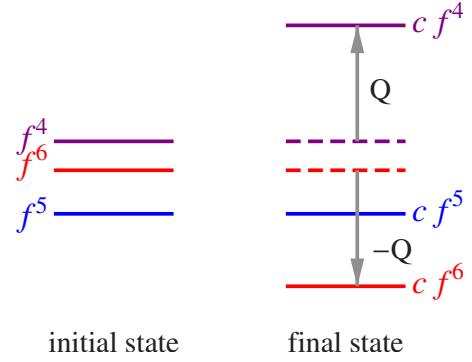
FIG. 4. (Color online) Energy level diagram for the configurations in the initial and final states before hybridization using the parameters obtained from a best fit to the experimental PE spectra: $\Delta=1.5$ eV, $U=4$ eV, and $Q=4$ eV, which corresponds to $E(5f^4)=2.5$ eV, $E(5f^5)=0$ eV, and $E(5f^6)=1.5$ eV for the ground state and $E(\underline{c}5f^4)=6.5$ eV, $E(\underline{c}5f^5)=0$ eV, and $E(\underline{c}5f^6)=-2.5$ eV for the final state. In the final state, the $5f^5$ and $5f^6$ configurations are reversed in energy compared to the ground state due to the large core-valence Coulomb interaction Q.

R_c (=0.6) and R_v (=0.8). Upon creation of a core hole c is created, the $5f$ wave function is contracted so that the hybridization strength V between $\underline{c}5f^4$ and $\underline{c}5f^5$ is reduced to $R_c V$. Furthermore, the hybridization between $5f^5$ and $5f^6$ is taken as V/R_v since the $5f$ wave function is more extended with increasing $5f$ electron number. The calculated PE lines are broadened by a Lorentzian of $\Gamma=0.2$ eV (half width at half maximum) to account for intrinsic line width (core-hole lifetime) and a Gaussian of $\sigma=0.3$ eV for instrumental broadening and the results are presented in Sec. IV.

IV. RESULTS AND DISCUSSION

The experimental $4f$ PE spectra of Pu, discussed in Sec. II, were fitted using the cluster model calculation described in Sec. III. Good overall agreement was obtained for fixed values $\Delta=1.5$ eV, $U=4$ eV, and $Q=4$ eV and varying the mixing parameter V for the different Pu thin films and allotropes. Δ, U, and Q determine the relative energies of the different configurations in the initial and final states [Eqs. (10) and (11)]. Figure 4 shows a schematic picture of the obtained relative energy positions for the configurations before hybridization. In the initial state, $5f^5$ is the lowest configuration with $5f^4$ and $5f^6$ at 2.5 eV and 1.5 eV higher energy, respectively. This is in good agreement with the calculation of Pu by Johansson and Rosengren, who showed that the f^5 configuration is stable compared to the f^4 and f^6 configurations with ~2.5 eV and ~1.5 eV, respectively.[12,27] In the final state, the $\underline{c}5f^6$ configuration is, with respect to the $\underline{c}5f^5$, pulled down in energy by an amount Q due to the core-valence Coulomb interaction. The energy difference between these two final-state configurations is $\Delta - Q = -2.5$ eV [cf., Eq. (11)]. A point to note, which is crucial for the screening, is that the relative energy positions of $5f^5$ and $5f^6$ are reversed in the final state compared to the ground state (cf., Fig. 4).
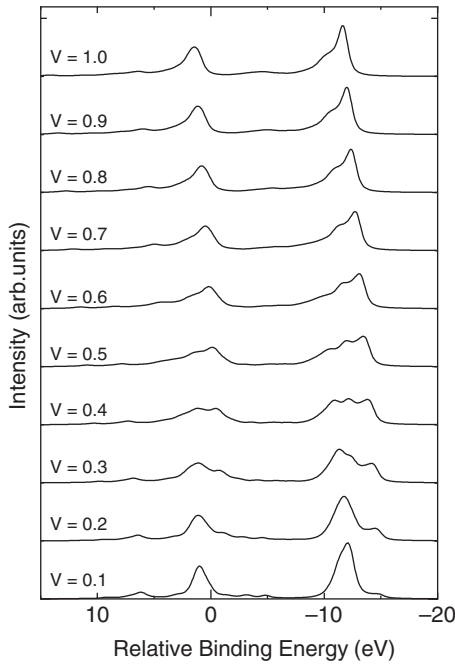
FIG. 5. Calculated $4f$ PE using Anderson impurity model with the transfer integral V varying from 0.1 to 1.0 eV and $\Delta = 1.5$ eV, $U = 4$ eV, and $Q = 4$ eV. The gradual energy shift of the spectra with V is due to a change in hybridization energy.

The spectra with V varied between 0.1 and 1.0 eV for the fixed values of Δ, U, and Q are shown in Fig. 5. The gradual energy shift of the spectra with V is due to a change in hybridization energy. Both the $4f_{7/2}$ and $4f_{5/2}$ structures consist of a broad manifold, where one can distinguish a peak at low BE and a peak structure at $\sim$3 eV higher BE. The relative intensity ratio of these features shows strong gradual changes as a function of V. For $V \leq 0.3$ the intensity of the low BE feature is small and increases quadratically with V. The low BE feature is clearly dominant for $V \geq 0.6$. As the $\underline{c}5f^6$ configuration has the lowest energy, the low BE peak has mainly $\underline{c}5f^6$ character and is the well screened peak. For weak screening (small V) the intensity of the well screened peak has low intensity while for strong screening (large V) the well screened peak has high intensity. This screening process is in agreement with the simple analytical model presented in Sec. III C.

In Fig. 6 we compare the experimental results for the 1, 2, 3, 5, and 9 ML Pu thin films with the calculated Pu $4f$ PE spectra for $V = 0.25$ eV, 0.35 eV, 0.4 eV, 0.45 eV, and 0.55 eV, respectively. In Fig. 7 the experimental results for Pu metal in δ and α phases are compared with the calculated spectra for $V = 0.55$ eV and 1.1 eV, respectively. In all cases there is a good agreement between calculated and measured spectra. Note that in the calculations we neglect any inelastic photoemission processes, such as represented by a Shirley background correction or an electron-energy-loss function. These processes are responsible for most of the "background" intensity above the peaks.

The calculated f weights (in percent) in the ground state, obtained from the $4f$ PE spectra shown in Figs. 6 and 7, are listed in Table II for the different Pu thin films and allot-
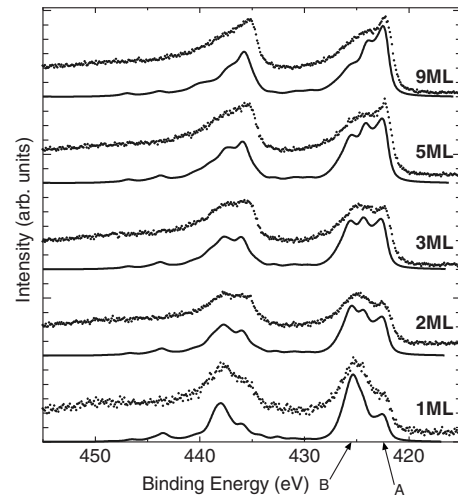
FIG. 6. The $4f$ PE for Pu thin films. Experimental results (dots) for 1, 2, 3, 5, and 9 ML (from Ref. 46) and calculations (drawn lines) for $V = 0.25$, 0.3.5, 0.4, 0.45, and 0.55 eV ($\Delta = 1.5$ eV, $U = 4$ eV, and $Q = 4$ eV), cf., Table II. The arrows A and B indicate the main and satellite peaks, respectively

ropes. The f weights are also graphically represented in Fig. 8, which shows their systematic change from localized to delocalized character in Pu metal. From the weights, we can derive the f count, $\langle n \rangle = \Sigma_n p_n n$, as well as the standard deviation, $\sigma = \Sigma_n p_n (n - \langle n \rangle)^2$, where p_n is the weight of f^n. These values are also shown in Table II.

The PE of δ Pu resembles the 9 ML Pu thin film, with $V = 0.55$ eV, whereas α Pu requires a much larger value V of 1.1 eV. Thus as one would expect, α Pu is more delocalized, resulting in f^4, f^5, and f^6 weights of $\sim$10%, 60%, and 30%, respectively. This is still far away from an itinerant model, where the probability that at an instantaneous moment an atom has n electrons is given by the binomial distribution in Eq. (1) and shown in Fig. 3. In this one-electron model an f count of 5.22 gives a very flat distribution over all configu-
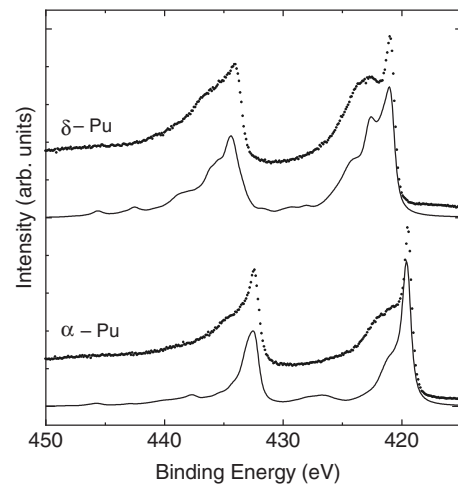
FIG. 7. The $4f$ photoemission for Pu metal in α and δ phases. Experimental results (dots) (from Ref. 48 and 49) and calculated results (drawn lines). Parameters used in the calculation can be found in Table II.

TABLE II. Ground-state $5f$ weights (in %) for the Pu films with different thickness and for α and δ Pu metal as obtained from the calculated $4f$ PE spectra shown in Figs. 6 and 7. The corresponding values of V are given (with $\Delta=1.5$ eV, $U=4$ eV, and $Q=4$ eV) together with the derived f count, $\langle n \rangle = \Sigma_n p_n n$, and standard deviation, $\sigma = \Sigma_n p_n (n - \langle n \rangle)^2$, where p_n is the weight of the $5f^n$ configuration.

	V (eV)	$5f^4$	$5f^5$	$5f^6$	$\langle n \rangle$	σ
1 ML	0.25	1.3	81.4	17.3	5.16	0.16
2 ML	0.35	2.6	74.7	22.7	5.20	0.21
3 ML	0.40	3.4	72.1	24.5	5.21	0.23
5 ML	0.45	4.2	69.9	25.9	5.22	0.25
9 ML	0.55	5.7	66.4	27.8	5.22	0.29
δ Pu	0.55	5.7	66.4	27.8	5.22	0.29
α Pu	1.1	9.6	58.8	31.6	5.22	0.36

rations from $n=0$ to 14, with f^4, f^5, and f^6 weights of 18.2%, 21.6%, and 19.2%, respectively, and a standard deviation $\sigma = 1.81$. However, taken only over the three configurations it gives a standard deviation $\sigma = 0.63$. Table I gives $\sigma = 0.36$ and 0.29 for α and δ-Pu metal, respectively.

It is interesting that in our model the f count is almost constant for the different Pu metals. Its value of 5.22 is the same for the α and δ phases of Pu metal and for layers ≥ 5 ML Pu, and for a 1 ML thin film reduces only to a slightly lower value of 5.16. The constant f count arises primarily from the fact that the relative energy positions of the different $5f^n$ configurations remain fixed. This means that Δ and U have the same value for the different Pu metals. In fact, independent of which calculational approach one is using, most theories conclude that the $5f$ occupation for all phases of Pu deviates less than 0.1 electron.[14,68,69]

The similar f count for α and δ Pu is in agreement with EELS measurement. Both allotropes have practically the same $N_{4,5}$ branching ratio, which means they have the same number of f electrons, assuming the angular momentum coupling does not change.[42]

The obtained values for the f weights can be compared with those reported by Cox et al.,[70] who modeled the Pu $4f$

PE using the Gunnarsson-Schönhammer approach[45] without taking into account the multiplet structure. Using $U = 4.4$ eV and $Q = 6$ eV, these authors find a more atomiclike ground state for both Pu allotropes, namely, 97% f^5 and 3% f^6 for δ Pu and 6% f^4, 88% f^5, and 6% f^6 for α Pu, hence yielding in both cases an f count of ~5. Because these authors do not include multiplet structure in their model calculation, the obtained valence fluctuations are smaller. Multiplet structure causes the levels to spread in energy, thereby increasing the mixing between nearby levels of different configurations. This demonstrates the importance of the presence of multiplet structure in the description for the fluctuating nature of the ground state.

Compared to the values for δ Pu in Table II, the LDA +DMFT calculations by Shim et al.[18] gives the same f count of 5.2 but with a more delocalized ground state of f^4, f^5, and f^6 weights around 8%, 62%, and 30%, respectively. This difference can be ascribed to the fact that our cluster model does not include band structure. However, LDA+DMFT calculations have so far only been performed for $5f$ valence PE and not for $4f$ PE, where the core hole breaks the translation symmetry.

V. CONCLUSIONS

The $4f$ core-level photoemission spectra of Pu metal exhibit screened and unscreened peaks which can be used as a measure for the degree of localization. Increased localization (more atomiclike) leads to decreased overlap which results in a volume increase. There is a competition between localization (electron-electron interaction) and delocalization (kinetic energy). The many-body crystal wave function has to reduce to many-body atomic wave functions as the lattice spacing is increased. Strongly correlated electron systems can be studied by an Anderson impurity model or by DMFT, where the intra-atomic Coulomb interaction and hybridization are considered at the same footing. Electron correlation effects depend on the lattice phase, e.g., when the distance between the atoms is small, the correlation effects may not be so important, since the hybridization, and consequently the bandwidth becomes large.

Using first a simple analytical model for a two-level system we show that an increase in the main peak with in-
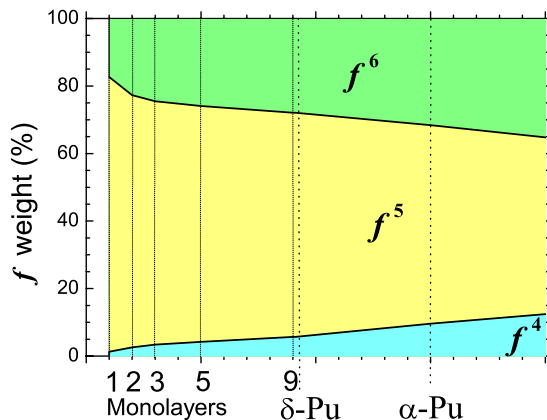
FIG. 8. (Color online) Graphical presentation of the distribution of $5f$ weights (in percent) in the ground state for the Pu films with different thickness and for α and δ Pu metal as obtained from $4f$ PE (values given in Table II).

creased mixing proves that the ground state has mainly $5f^5$ character instead of $5f^6$. Since for Pu we find that $Q > \Delta$, the well screened peak is the main peak, i.e., has the lowest energy, and for small hybridization the main to satellite peak intensity increases with the square of the mixing.

The Pu $4f$ photoemission spectra are analyzed using an Anderson impurity model including full multiplet structure, where we obtain the on-site Coulomb interaction U and the $5f$ weights under the assumption that the core-ionized atom can be described as an impurity state. An Anderson impurity model is justified as long as the mixing (hybridization) between the different $5f^n$ configurations is small compared to their energy separation. From comparison with the $4f$ PE, we obtain a value for the $5f$ Coulomb interaction $U=4$ eV for Pu metal. This is an important experimental verification of the theoretical value of 4.0–4.5 eV used in the LDA +DMFT approach[18,20,28,29,71] that explains the equilibrium volume, the paramagnetism,[18] $5f$ photoemission,[18,29] linear specific heat,[30] and phonon spectrum.[72] Moreover, also the values obtained for the relative energies of the different $5f^n$ configurations agree well with the calculated values by Johansson and Rosengren.[12]

The observed changes in the Pu $4f$ photoemission are very well reproduced by the Anderson impurity model calculation, where the main peak structure is due to well screened $\underline{c}5f^6$ states and the satellite structure is caused by poorly screened $\underline{c}5f^5$ states. For 1 ML Pu, most of the intensity is in the satellite peak, whereas for 9 ML Pu the intensity has mostly shifted to the main peak. The calculation gives an f count of 5.22 with only a minor gradual change for ultrathin films. The obtained f count disagrees with LDA+U calculations that come up with close to six $5f$ electrons for δ Pu (Refs. 15–17) but is fully in agreement with recent LDA +DMFT calculations[18] and with recent results from the branching-ratio analysis in EELS and XAS.[3]

The strong changes in the PE spectral shape can be explained by a gradual change in mixing (hybridization) of the $5f$ states with adjacent orbitals as a function of localization. This change in mixing has important consequences for the fluctuations in the $5f$ electron distribution, showing that the $5f$ states become more localized in thinner films. The result for δ Pu is similar as for the 9 ML film but is quite different than for α Pu. While for both phases the f count is the same, the mixing of the $5f$ electrons in the α phase is twice that of the δ phase, as might be expected from the more delocalized $5f$ state in α Pu metal. We demonstrate the importance of including the full multiplet structure in the Anderson impurity model calculation to obtain an appropriate description of the valence fluctuations in the partly localized material. Further improvements can be made by taking also into account band dispersion. However, such calculations have so far not been done in the presence of a core hole.

The results confirm that the $5f$ localization increases for thinner layers, which causes the shape of the f orbital to change to a less overlapping orbital. Therefore if the possibility of magnetism, which has always been anticipated but never observed in Pu metal, is realized, it would be for the thinnest films, where the localization is strongest due to reduced hybridization.[10] This effect should be distinguished from the magnetic-moment formation that occurs for Pu impurities in palladium alloys which is driven by the charge transfer.[73]

[1] J. P. Desclaux and A. J. Freeman, *Handbook on the Physics and Chemistry of the Actinides* (Elsevier, Amsterdam, 1984), Vol. I.

[2] P. Söderlind, Adv. Phys. **47**, 959 (1998).

[3] K. T. Moore and G. van der Laan, Rev. Mod. Phys. **81**, 235 (2009).

[4] P. Santini, S. Carretta, G. Amoretti, R. Caciuffo, N. Magnani, and G. H. Lander, Rev. Mod. Phys. **81**, 807 (2009).

[5] B. Johansson and H. Skriver, J. Magn. Magn. Mater. **29**, 217 (1982).

[6] S. Heathman, R. G. Haire, T. L. Bihan, A. Lindbaum, M. Idiri, P. Normile, S. Li, R. Ahuja, B. Johansson, and G. H. Lander, Science **309**, 110 (2005).

[7] K. T. Moore, G. van der Laan, R. G. Haire, M. A. Wall, A. J. Schwartz, and P. Söderlind, Phys. Rev. Lett. **98**, 236402 (2007).

[8] S. S. Hecker, Mater. Res. Bull. **26**, 672 (2001).

[9] S. S. Hecker, D. R. Harbur, and T. G. Zocco, Prog. Mater. Sci. **49**, 429 (2004).

[10] G. van der Laan and K. T. Moore, in *Magnetism and Synchrotron Radiation*, Springer Proceedings in Physics Vol. 133, edited by E. Beaurepaire (Springer-Verlag, Berlin, 2010), pp. 313–344.

[11] H. A. Dürr, G. van der Laan, D. Spanke, F. U. Hillebrecht, and N. B. Brookes, Phys. Rev. B **56**, 8156 (1997).

[12] B. Johansson and A. Rosengren, Phys. Rev. B **11**, 1367 (1975).

[13] Y. G. Hao, O. Eriksson, G. W. Fernando, and B. R. Cooper, Phys. Rev. B **43**, 9467 (1991).

[14] P. Söderlind, J. M. Wills, B. Johansson, and O. Eriksson, Phys. Rev. B **55**, 1997 (1997).

[15] A. O. Shorikov, A. V. Lukoyanov, M. A. Korotin, and V. I. Anisimov, Phys. Rev. B **72**, 024458 (2005).

[16] A. B. Shick, V. Drchal, and L. Havela, Europhys. Lett. **69**, 588 (2005).

[17] L. V. Pourovskii, M. I. Katsnelson, A. I. Lichtenstein, L. Havela, T. Gouder, F. Wastin, A. B. Shick, V. Drchal, and G. H. Lander, Europhys. Lett. **74**, 479 (2006).

[18] J. H. Shim, K. Haule, and G. Kotliar, Nature (London) **446**, 513 (2007).

[19] A. Georges, G. Kotliar, W. Krauth, and M. J. Rozenberg, Rev. Mod. Phys. **68**, 13 (1996).

[20] S. Y. Savrasov, G. Kotliar, and E. Abrahams, Nature (London) **410**, 793 (2001).

[21] G. Kotliar, S. Y. Savrasov, K. Haule, V. S. Oudovenko, O. Parcollet, and C. A. Marianetti, Rev. Mod. Phys. **78**, 865 (2006).

[22] J. C. Lashley, A. Lawson, R. J. McQueeney, and G. H. Lander, Phys. Rev. B **72**, 054416 (2005).

[23] R. H. Heffner *et al.*, Phys. Rev. B **73**, 094453 (2006).

[24] N. J. Curro and L. Morales, Mater. Res. Soc. Symp. Proc. **802**, 53 (2004).

[25] Y. Piskunov, K. Mikhalev, A. Gerashenko, A. Pogudin, V. Ogloblichev, S. Verkhovskii, A. Tankeyev, V. Arkhipov, Y. Zouev, and S. Lekomtsev, Phys. Rev. B **71**, 174410 (2005).

[26] A. B. Shick, J. Kolorenc, L. Havela, V. Drchal, and T. Gouder, EPL **77**, 17003 (2007).

[27] T. Björkman, O. Eriksson, and P. Andersson, Phys. Rev. B **78**, 245101 (2008).

[28] S. Y. Savrasov and G. Kotliar, Phys. Rev. Lett. **84**, 3670 (2000).

[29] J.-X. Zhu, A. K. McMahan, M. D. Jones, T. Durakiewicz, J. J. Joyce, J. M. Wills, and R. C. Albers, Phys. Rev. B **76**, 245118 (2007).

[30] L. V. Pourovskii, G. Kotliar, M. I. Katsnelson, and A. I. Lichtenstein, Phys. Rev. B **75**, 235107 (2007).

[31] O. Eriksson, J. D. Becker, A. V. Balatsky, and J. M. Wills, J. Alloys Compd. **287**, 1 (1999).

[32] J. M. Wills, O. Eriksson, A. Delin, P. H. Andersson, J. J. Joyce, T. Durakiewicz, M. T. Butterfield, A. J. Arko, D. P. Moore, and L. A. Morales, J. Electron Spectrosc. Relat. Phenom. **135**, 163 (2004).

[33] A. Svane, L. Petit, Z. Szotek, and W. M. Temmerman, Phys. Rev. B **76**, 115116 (2007).

[34] P. W. Anderson, Phys. Rev. **124**, 41 (1961).

[35] J. Hubbard, Proc. R. Soc. London, Ser. A **276**, 238 (1963).

[36] J. Hubbard, Proc. R. Soc. London, Ser. A **277**, 237 (1964).

[37] B. T. Thole and G. van der Laan, Phys. Rev. A **38**, 1943 (1988).

[38] B. T. Thole and G. van der Laan, Phys. Rev. B **38**, 3158 (1988).

[39] G. van der Laan and B. T. Thole, Phys. Rev. Lett. **60**, 1977 (1988).

[40] G. van der Laan and B. T. Thole, Phys. Rev. B **53**, 14458 (1996).

[41] G. van der Laan, K. T. Moore, J. G. Tobin, B. W. Chung, M. A. Wall, and A. J. Schwartz, Phys. Rev. Lett. **93**, 097401 (2004).

[42] K. T. Moore, G. van der Laan, R. G. Haire, M. A. Wall, and A. J. Schwartz, Phys. Rev. B **73**, 033109 (2006).

[43] J. R. Naegele, L. Manes, J. C. Spirlet, and W. Müller, Phys. Rev. Lett. **52**, 1834 (1984).

[44] G. van der Laan, C. Westra, C. Haas, and G. A. Sawatzky, Phys. Rev. B **23**, 4369 (1981).

[45] O. Gunnarsson and K. Schönhammer, Phys. Rev. B **28**, 4315 (1983).

[46] T. Gouder, L. Havela, F. Wastin, and J. Rebizant, Europhys. Lett. **55**, 705 (2001).

[47] A. J. Arko, J. J. Joyce, L. A. Morales, J. H. Terry, and R. K. Schulze, *Challenges in Plutonium Science* (Los Alamos Science, Los Alamos, NM, 2000), Vol. 1, pp. 168-185.

[48] J. Terry, R. K. Schulze, J. D. Farr, T. Zocco, K. Heinzelman, E. Rotenberg, D. K. Shuh, G. van der Laan, D. A. Arena, and J. G. Tobin, Surf. Sci. **499**, L141 (2002).

[49] J. G. Tobin, B. W. Chung, R. K. Schulze, J. Terry, J. D. Farr, D. K. Shuh, K. Heinzelman, E. Rotenberg, G. D. Waddill, and G. van der Laan, Phys. Rev. B **68**, 155109 (2003).

[50] J. C. Fuggle, M. Campagna, Z. Zolnierek, R. Lässer, and A. Platau, Phys. Rev. Lett. **45**, 1597 (1980).

[51] H. R. Moser, B. Delley, W. D. Schneider, and Y. Baer, Phys. Rev. B **29**, 2947 (1984).

[52] J. R. Naegele, L. E. Cox, and J. W. Ward, Inorg. Chim. Acta **139**, 327 (1987).

[53] S. Doniach and M. Sunjic, J. Phys. C **3**, 285 (1970).

[54] L. I. Johansson, J. W. Allen, I. Lindau, M. H. Hecht, and S. B. M. Hagström, Phys. Rev. B **21**, 1408 (1980).

[55] W. McLean, C. A. Colmenares, R. L. Smith, and G. A. Somorjai, Phys. Rev. B **25**, 8 (1982).

[56] J. C. Fuggle, F. U. Hillebrecht, Z. Zolnierek, R. Lässer, C. Freiburg, O. Gunnarsson, and K. Schönhammer, Phys. Rev. B **27**, 7330 (1983).

[57] R. Baptist, D. Courteix, J. Chayrouse, and L. Heintz, J. Phys. F: Met. Phys. **12**, 2103 (1982).

[58] G. van der Laan, J. Zaanen, G. A. Sawatzky, R. C. Karnatak, and J. M. Esteva, Phys. Rev. B **33**, 4253 (1986).

[59] G. van der Laan, S. S. Dhesi, and E. Dudzik, Phys. Rev. B **61**, 12277 (2000).

[60] G. van der Laan, E. Arenholz, E. Navas, A. Bauer, and G. Kaindl, Phys. Rev. B **53**, R5998 (1996).

[61] G. van der Laan, E. Arenholz, E. Navas, Z. Hu, E. Mentz, A. Bauer, and G. Kaindl, Phys. Rev. B **56**, 3244 (1997).

[62] W. J. Lademan, A. K. See, L. E. Klebanoff, and G. van der Laan, Phys. Rev. B **54**, 17191 (1996).

[63] G. Panaccione, G. van der Laan, H. A. Dürr, J. Vogel, and N. B. Brookes, Eur. Phys. J. B **19**, 281 (2001).

[64] G. van der Laan and B. T. Thole, Phys. Rev. B **48**, 210 (1993).

[65] R. D. Cowan, *The Theory of Atomic Structure and Spectra* (University of California Press, Berkeley, 1982).

[66] G. van der Laan, Lect. Notes Phys. **697**, 143 (2006).

[67] B. T. Thole, G. van der Laan, J. C. Fuggle, G. A. Sawatzky, R. C. Karnatak, and J. M. Esteva, Phys. Rev. B **32**, 5107 (1985).

[68] O. Eriksson, L. E. Cox, B. R. Cooper, J. M. Wills, G. W. Fernando, Y. G. Hao, and A. M. Boring, Phys. Rev. B **46**, 13576 (1992).

[69] J. van Ek, P. A. Sterne, and A. Gonis, Phys. Rev. B **48**, 16280 (1993).

[70] L. E. Cox, J. M. Peek, and J. W. Allen, Physica B **259-261**, 1147 (1999).

[71] C. A. Marianetti, K. Haule, G. Kotliar, and M. J. Fluss, Phys. Rev. Lett. **101**, 056403 (2008).

[72] X. Dai, S. Y. Savrasov, G. Kotliar, A. Migliori, H. Ledbetter, and E. Abrahams, Science **300**, 953 (2003).

[73] W. J. Nellis and M. B. Brodsky, Phys. Rev. B **4**, 1594 (1971).